and by the statics of the counts in the samples. Figure 2 shows typical on-orbit performance. The data were obtained on August 26, 1990 and consist of 60-s averages of raw count rates in alternate channels, beginning with the lowest energy channel (Ch 0). The plot starts at perigee below the particle trapping region of the magnetosphere, goes up through the inner zone, through the slot, and out into the outer zone. Just after 20,000 s UT, a minor magnetic storm occurs. The effect on the energetic electrons is quite evident. The vehicle then goes back through the slot and into the inner zone. At that point the vehicle was put into a LASSII mode and the MEA data stopped. The data have not been corrected for proton contamination in the inner zone.

Acknowledgments

Construction and integration of this instrument was funded under Air Force Space Systems Division Contract F0471-88-089. The authors thank G. Boyd, D. Chennette, J. Cowder, C. Holmes, S. Imamoto, N. Katz, R. Koga, and P. Lew, all of whom contributed significantly to the successful on-orbit operation of this instrument.

References

[1]Siegbahn, K. (ed.), *Beta- and Gamma-Ray Spectroscopy,* Interscience, New York, 1955, pp. 52–99.

[2]Koga, R., Imamoto, S. S., Katz, N., and Pinkerton, S. D., "Data Processing Units for Eight Magnetospheric Particle and Field Sensors," *Journal of Spacecraft and Rockets,* Vol. 29, No. 4, 1992, pp. 574–579.

Proton Switches

J. B. Blake* and S. S. Imamoto†
The Aerospace Corporation, Los Angeles, California 90009

THE proton switches (PS) are two omnidirection detectors, sensitive to protons (and heavier ions). The name proton switch has an historical origin. They were used in a mission 20 years ago (OV1-20PM) for turning on a high-power payload when energetic protons were present, and turning it off when the proton flux dropped below a preset value. In its first incarnation SPACERAD was to have been a simple, duty-cycled payload.

The PS detectors are Li-drifted silicon with a cubical shape, 3 mm on an edge. A uniform hemispherical shield is placed over the upper 2π solid angle; the rear 2π solid angle is shielded far more massively. The configuration is shown in Fig. 1. The detectors are connected to the usual preamplifier, amplifier, and discriminator electronic systems. The discriminator levels are chosen to be several times the energy which an electron can deposit in the detector. As a result, only protons and heavier ions are detected, and background caused by electron pileup is nil. The energy threshold is determined by the thickness of the hemispherical shield and, to a much smaller degree, by the discriminator thresholds. The hemispherical shields for the SPACERAD sensors were chosen to be 20 MeV and 50 MeV (for protons).

A zeroth-order estimate of the geometric factor is computed in the following way. The efficiency $\epsilon(E,E_B)$ is calculated from proton range-energy tables and geometric considerations, i.e., the path-length distribution converted to energy deposit for a given discriminator level E_B. The geometric factor is defined by the following expression:

$$\bar{\epsilon}\int_{E_l}^{E_u} e^{-E/E_0} = \int_{E_l}^{E_u} \epsilon(E,E_B)e^{-E/E_0}$$

where the subscripts l and u refer to the lower and upper limits of the energy channel. The lower level E_l is fixed by the shield and E_B is set by the electronic threshold. Therefore the integration given above is carried out for values of E_0 of geophysical interest and for a series of values for E_u. The value of E_u is selected such that the geometric factor is independent of the spectral index. Similar calculations have been carried out for power-law spectra; the results are much the same. Table 1 gives the geometric factor for the four PS channels for exponential spectra.

It is important to note the assumption that goes into the calculations of geometric factor and energy passband—that the spectral shape is either exponential or power-law and fixed over the entire energy range of integration. In the inner zone, it is conventional wisdom that the proton spectra are exponentials over a large energy range, cf. AP-8. In the case of solar-flare spectra, this assumption usually is not a good one. *The geometric factors and passbands are gross approximations only, and must be used with care.*

A conversion of count rate to proton flux can be made readily by using the large arrays of calculated values for $\epsilon(E,E_B)$; this must be done for quantitative work. (The calculated efficiencies as a function of energy are available from the authors.) However, the major purpose for including these two sensors in the SPACERAD payload was to provide guidance in the analysis of the data from the more sophisticated sensors—is there a penetrating proton background, about how large is it, and what roughly is the spectral shape? These purposes are well served by the information in Table 1.

It was noted above that these sensors have no electron sensitivity. However, they do show a very low count rate due to galactic cosmic rays. Since there are very few cosmic rays in the passbands of the proton switches, the major causes of these background counts are nuclear interactions in the detector itself and neutron-induced reactions in the detector where the neutrons are secondaries generated in the spacecraft. This low cosmic-ray background varies over the combined release and radiation effects satellite (CRRES) orbit because of the variations in geomagnetic cutoff.

Figure 2 is a line plot of the output of the two sensors for a partial orbit including the inner zone where the trapped energetic protons are found. The upper trace is for the sensor with the 20-MeV shield (lower energy threshold); the lower one for the 50-MeV shield (lower energy threshold). This figure clearly shows the sensor characteristics described above. Note the immunity to background counts from electrons; away from the broad peaks due to the inner zone protons only the very low residual galactic cosmic-ray background can be seen. It also is easy to see that near perigee (34,999–35,000 s), where many of the galactic cosmic rays are excluded by the Earth's magnetic field, the background rate indeed is significantly reduced compared to the background count rate seen elsewhere.

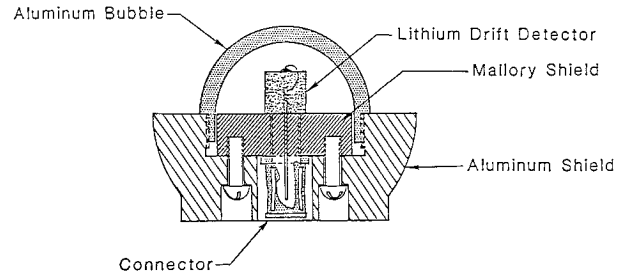

Fig. 1 A cross section of a proton switch sensor is shown with the key components labeled.

Received June 6, 1991; revision received Aug. 9, 1991; accepted for publication Aug. 9, 1991.

*Director, Space Particles and Fields Department, Space and Environmental Technology Center, P.O. Box 92957.

†Research Engineer, Space Particles and Fields Department, Space and Environmental Technology Center, P.O. Box 92957.

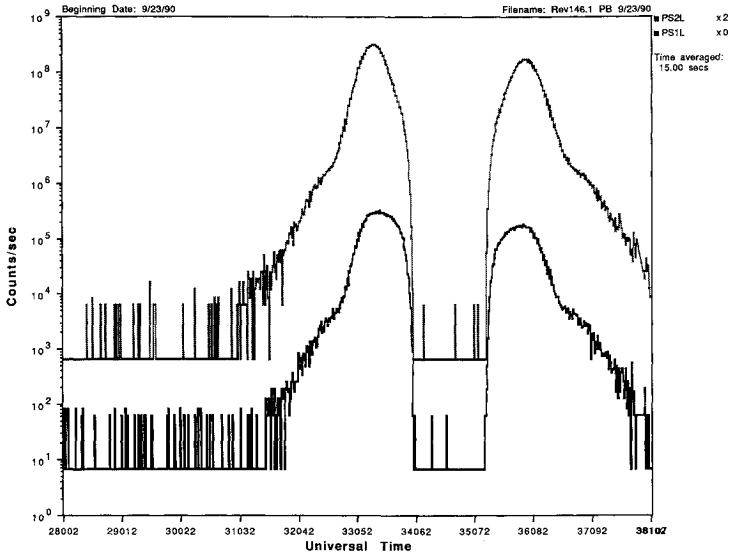

Fig. 2 Data from the low-threshold channels of the two proton switches are shown during the time period around perigee. Note that the top curve is multiplied by 100 in order to separate the two curves. Between ≈ 28,000 and 31,500 s the CRRES spacecraft was above the region containing the energetic protons, and the proton switches were counting cosmic-ray background. The two peaks result from the inbound and outbound legs of the CRESS orbit because the spacecraft goes below the radiation belts before reaching perigee. Note the very low background between the peaks (around perigee) where the geomagnetic field excludes much of the galactic cosmic-ray flux; thus the background count rate is reduced substantially in that region.

Table 1 Calculated approximate geometric factors and energy ranges

Channel identification	Energy range, MeV	Geometric factor, mm^2
PS2L	21-84	3.9
PS2H	23-51	2.6
PS1L	51-107	3.6
PS1H	51-77	2.7

Acknowledgment

This work was supported under Air Force Space Systems Division Contract FO4701-88-0089.

CRRES Low-Energy Magnetospheric Ion Composition Sensor

D. T. Young*
Southwest Research Institute
San Antonio, Texas 78228
and
B. L. Barraclough,† D. J. McComas,†
M. F. Thomsen,† K. McCabe,‡
and R. Vigil‡
Los Alamos National Laboratory
Los Alamos, New Mexico 87545

Introduction

ONE major goal of space plasma physics is understanding the origins, acceleration processes, and transport of mass, momentum, and energy through the Earth's magnetosphere, objectives that are addressed by plasma mass spectrometry. Both the solar wind, consisting predominantly of H^+ and $^4He^{2+}$ ions, and the terrestrial topside ionosphere, which consists primarily of H^+, He^+, O^{2+}, and O^+, contribute to magnetospheric particle populations. Furthermore, many acceleration processes are dependent on the ion mass/charge ratio, as are transport and loss processes.[1,2] The low-energy magnetospheric ion composition spectrometer (LOMICS) instrument described here is designed to distinguish and measure the velocity distributions of all important magnetospheric ion species up to 44 keV per charge.

Instrumental Approach

Most mass spectrometer experiments flown previously on spacecraft have been based on magnetic analysis of ion momentum (see Ref. 3 and references therein). This technique has several practical limitations, most notably an upper limit on ion energy of about 20 keV, as well as limits on time resolution caused by the need to scan the mass spectrum. More recently, time-of-flight (TOF) methods have been used to obtain solar wind, cometary, and magnetospheric composition measurements,[4,5] usually with emphasis at energies above several tens of kilaelectron volts. LOMICS' TOF technique represents an attempt to improve on limitations of both magnetic and earlier TOF devices, and yet still produce a compact instrument capable of high-quality measurements. It is important to keep in mind that the LOMICS design was also constrained by pre-existing restrictions on volume, mass, and power, and by the design of pre-existing high-voltage power supplies.

Instrument Description

Figure 1 is a schematic diagram of the LOMICS sensor. The sensor is mounted, together with the heavy ion telescope (HIT)[6] and their common data processing unit (DPU)[7] and power supplies, in the high-mass sensor-B (HMSB) unit. Microchannel plate (MCP) detectors and other sensitive elements in LOMICS were protected by a hermetically sealed housing and aperture cover. The cover was opened on-orbit four weeks after launch, when spacecraft outgassing was judged to be acceptably low.

LOMICS consists of a conventional 90-deg spherical-section electrostatic analyzer (ESA) followed by a TOF analyzer. The ESA provides ion energy/charge (E/Q) and angular anal-

Received June 21, 1991; revision received Aug. 27, 1991; accepted for publication Sept. 2, 1991.

*Institute Scientist, Department of Space Sciences, Instrumentation and Space Research Division, P.O. Drawer 28510.

†Staff Member, Space Plasma Physics Group, Space Science and Technology Division, Mail Stop D438.

‡Staff Member, Space Instrumentation Group, Space Science and Technology Division, Mail Stop D440.